Carbon 121 (2017) 380–388

Contents lists available at ScienceDirect

Carbon

journal homepage: www.elsevier.com/locate/carbon

Formation of incipient soot particles from polycyclic aromatic hydrocarbons: A ReaxFF molecular dynamics study

Qian Mao [a, b], Adri C.T. van Duin [b, *], K.H. Luo [a, c, **]

[a] Center for Combustion Energy, Key Laboratory for Thermal Science and Power Engineering of Ministry of Education, Department of Thermal Engineering, Tsinghua University, Beijing 100084, China
[b] Department of Mechanical and Nuclear Engineering, The Pennsylvania State University, University Park, PA 16802, USA
[c] Department of Mechanical Engineering, University College London, Torrington Place, London WC1E 7JE, UK

ARTICLE INFO

Article history:
Received 18 February 2017
Received in revised form
31 May 2017
Accepted 2 June 2017
Available online 3 June 2017

Keywords:
Polycyclic aromatic hydrocarbon (PAH)
Soot
Nucleation
ReaxFF
Molecular dynamics (MD)

ABSTRACT

In this study, we present the results from a series of ReaxFF molecular dynamics (MD) simulations to uncover the underlying mechanisms behind the nucleation and growth of incipient soot particles from polycyclic aromatic hydrocarbons (PAHs). PAHs, namely, naphthalene, anthracene, pyrene, coronene, ovalene and circumcoronene, are selected for ReaxFF MD simulations over a range of temperatures from 400 to 2500 K. Distinctive mechanisms of incipient soot formation are identified with respect to PAH mass and temperature. At low temperatures (e.g., 400 K), all types of the above PAHs can nucleate into incipient soot particles in stacked structures due to physical interactions. With the increase of temperature, the possibility of physical nucleation decreases for each PAH. At moderate temperatures (e.g., 1600 K), it becomes difficult for these PAH monomers, except circumcoronene grows into incipient soot particles. When the temperature increases to 2500 K, all the PAHs become chemically active, which not only leads to the formation of incipient soot particles but also takes the graphitization with the increase of the carbon-to-hydrogen (C/H) ratios in the particles. In addition to the formation of fullerene-like soot particles, stacked particles connected by 'carbon bridges' are also observed for large PAHs like coronene, ovalene and circumcoronene.

1. Introduction

Carbon materials, including zero-dimensional (0D) fullerenes, 1D nanotubes, 2D graphene and 3D graphite, are commercially produced in high-temperature aerosol environment by flame synthesis [1] and attract extensive attention in the materials science and condensed-matter physics [2]. At the same time, soot, composed of impure carbon, is generated from incomplete combustion of hydrocarbons and fossil fuels, which has a detrimental impact on the combustion efficiency [3], atmospheric visibility [4], and human health [5,6]. For both kinds of carbon-based materials, which are typically generated in high-temperature environments, it is accepted that nucleation is the starting point of the whole gas-to-particle conversion process [1,7]. Unfortunately, this nucleation process is currently poorly understood. Based on abundant numerous experimental studies, polycyclic aromatic hydrocarbons (PAHs) are widely accepted to be the precursors for fullerenes, graphite and soot [8–10]. Currently, there are three postulated soot nucleation paths [7], namely physical nucleation of PAHs into stacked clusters [11,12], chemical nucleation of PAHs into cross-linked three-dimensional structures [13,14] and generation of fullerene-like structures [15]. Though the above mechanisms all contribute to soot nucleation in flames, their relative importance or feasibility at different temperatures is still unclear. Due to the highly complex nature of soot inception, in recent soot modeling efforts [16,17], typically only the physical dimerization of PAH is taken into account for soot nucleation.

From an experimental perspective, determination of the low number density and short-lived PAHs is very difficult via laboratory methods [7], let alone detailed in-situ observation of soot nucleation and further growth. The complexity of the chemical and physical reactions during soot nucleation, makes it both numerically and experimentally challenging. Previous studies of the

* Corresponding author. Department of Mechanical and Nuclear Engineering, The Pennsylvania State University, University Park, PA 16802, USA.
** Corresponding author. Department of Mechanical Engineering, University College London, Torrington Place, London WC1E 7JE, UK.
E-mail addresses: acv13@engr.psu.edu (A.C.T. van Duin), K.Luo@ucl.ac.uk (K.H. Luo).

http://dx.doi.org/10.1016/j.carbon.2017.06.009

physical nucleation of soot are performed utilizing atomic simulation methods, such as density functional theory (DFT) calculations [7,18,19], molecular dynamics (MD) simulations [20–26] and Monte Carlo (MC) simulations [27]. Besides the dispersive and electrostatic forces [11], localized π-electron states in aromatic molecules are also reported to contribute to the PAH dimerization by DFT calculations [7,18,19]. Compared to DFT, MD is more capable to cover a wider range of mass distribution and to shed light on issues involving formation of incipient soot particles from PAH monomers. Frenklach et al. [12] utilized MD with the on-the-fly quantum forces to study the physical dimerization of PAHs and concluded that the energy transferring from translational energy to internal rotational and vibrational energy helps to extend the lifetime of dimers. Violi et al. [20–22] conducted MD simulations to investigate the growth of dimers to clusters and suggested that the aliphatic chains attached to aromatic sites facilitate the growth of soot particles at high temperatures. In the MD simulations performed by Kraft's group [23–25], a transferable anisotropic potential for PAHs was developed to study the physical nucleation of PAHs into soot particles and size-dependent melting of PAH clusters [26]. In addition, Rapacioli et al. [27] reported that stacked PAH conformation is the most stable based on MC simulations. All above MD and MC simulations are based on semi-empirical or empirical force fields that only describe physical nucleation. However, incipient soot particles comprised of PAHs by chemical bonds are also ubiquitous at temperatures above 1500 K as reported by D′ Anna in the opposed-flow ethylene flame [28]. Therefore, an alternative simulation method is desirable to overcome the limitations of the simulation time and the atom number in quantum mechanics (QM) simulations as well as the rigid connectivity between atoms in classical MD and MC simulations. ReaxFF MD is developed to describe the dynamic process involving both physical and chemical reactions for large systems at the atomic level with affordable computational cost [29]. In this paper, we utilize the ReaxFF MD to investigate the soot nucleation and growth from PAHs of different masses at varied temperatures. By examining the sizes of soot particles and tracing the structural evolutions, we are able to divulge the underlying soot nucleation mechanisms of temperature and PAH mass dependence.

2. Methodology

2.1. Simulation method

The ReaxFF force field is based on bond order/bond length [31,32] and parameterized against QM-based training sets. The ReaxFF force field includes the following energy components:

$$E_{system} = E_{bond} + E_{over} + E_{under} + E_{lp} + E_{val} + E_{tor} + E_{vdWaals} + E_{Coulomb} \quad (1)$$

where terms on the right-hand-side of the equation represent bond energy, over-coordination energy penalty, under-coordination stability, lone pair energy, valence angle energy, torsion angle energy, van der Waals energy, and coulomb energy, respectively. Charge equilibration (QEq) is performed to adjust the partial charge on individual atoms. A more detailed description of ReaxFF energy terms can be found in the literature [29]. On account of the accuracy, ReaxFF force field is similar or better than Parameterized Model number 3 (PM3). As for the computational cost, ReaxFF is about 100 times faster than PM3 and 10000 times faster than DFT calculations [28]. The ReaxFF C/H/O description in this paper was developed by incorporating $ReaxFF_{CHO}$ [29] and $ReaxFF_{C\text{-}2013}$ [33] to describe the reactions especially for thermal decomposition and C–C bond formation of large hydrocarbons like graphene and fullerene. More specifically, the $ReaxFF_{CHO}$ [29] is firstly developed through deriving from quantum chemical calculations on bond dissociation and reactions of small hydrocarbons molecules plus heat of formation, geometry data. The $ReaxFF_{C\text{-}2013}$ [33] is obtained by fitting against C–C bond dissociation, valence and torsion angle distortion, charges, and reaction energies. Up to now, this ReaxFF C/H/O description has been successfully incorporated with Ni, Si and noble gas ion (He^+, Ne^+, Ar^+, and Kr^+) to study nucleation of carbon nanotube from hydrocarbon precursors [34], high-kinetic energy collisions of nanoparticles and noble gas ions with graphene [35,36]. The similarity between graphene and PAH [37] indicates that the ReaxFF C/H/O force field should be capable of describing thermal and chemical properties of PAHs. The parameter sets for C/H/O description can be found in the supplementary material.

2.2. Simulation procedures

According to the mass spectra of high-molecular weight species in flames, PAH monomers are detected with mass ranging from about 100 to 700 amu [38] with carbon-to-hydrogen (C/H) ratio of 1.4–2.5 [39]. Therefore, PAHs constituted of 2-, 3-, 4-, 7-, 10-, and 19- numbered aromatic rings are selected and investigated in this study. The corresponding structures of PAH monomers are displayed in Fig. 1. Before MD simulations, the structure of each PAH monomer is minimized via a conjugate gradient algorithm. Each of the minimized PAH monomers is duplicated 50 times and then randomly distributed in a cubic box of 100 × 100 × 100 $Å^3$. Subsequently, a system energy minimization is performed. Then interactions between PAH monomers in a system are eliminated and the vibrational equilibrium of every monomer is performed to the specified simulation temperature for 1×10^6 iterations with a time step of 0.25 fs, while the translational and rotational components of the monomer are kept zero. In experiments, the well-distributed translational and rotational velocities come from sufficient

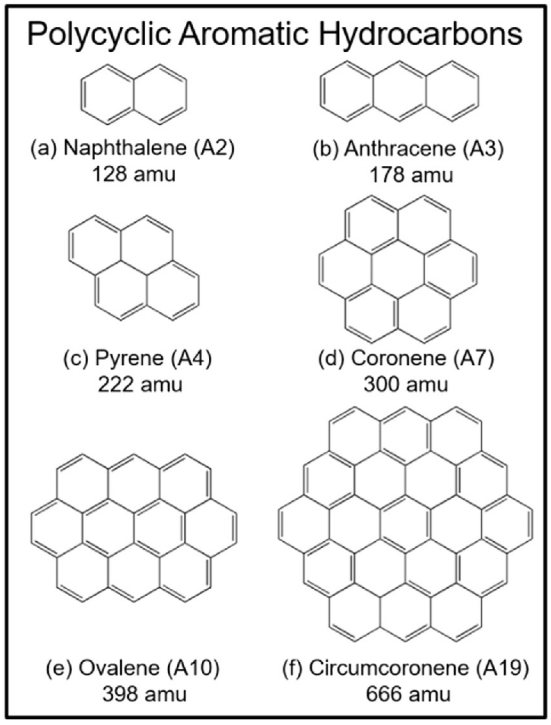

Fig. 1. Structures of the PAH monomers studied in ReaxFF MD simulations.

collisions with surrounding molecules, which, however, is difficult to achieve within the limited durations in MD simulations. Thus, based on the principle of equipartition of energy, the translational and rotational velocities of PAH monomers are given in Maxwellian distributions of the specified temperature. Details of distributing the translational and rotational velocities among PAHs in a system at a certain temperature can be found in the supplementary material.

Afterwards, dynamic processes of soot nucleation from different types of PAH are performed in the constant temperature canonical ensemble (NVT). Simulation temperatures are chosen at 400, 800, 1200, 1600, 2000 and 2500 K. Each simulation takes 8×10^6 iterations with a time step of 0.25 fs, which accounts for a total simulation time of 2 ns. Compared to the *ab initio* MD simulations performed by Frenklach et al. [12], classical MD simulations by Violi et al. [20] and Kraft et al. [23], our ReaxFF MD simulations overcome the limitations of the simulation duration, atom number as well as temperature range (above 1600 K). The Nosé-Hoover thermostat with a damping constant of 100 fs is adopted to control the system temperature. All the simulations are repeated for three times with different initial conformations to evaluate statistical relevance. MD simulations are performed using ReaxFF force field, which is implemented in the Large-scale Atomic/Molecular Massively Parallel Simulator (LAMMPS) package [40]. Snapshots and movies in this study are prepared by the Visual Molecular Dynamics (VMD) software [41].

2.3. Post-processing method

For incipient soot particles comprised of PAHs with chemical bonds, it is relatively easy to identify them from the atomic connection tables. However, for physical binding, an appropriate criterion to distinguish soot particles from PAH monomers is desirable. Dimerization of PAH monomers leads to stacked, T-shaped, 'shifted graphite' as well as crossed conformations [23], though stacking the PAH molecules yields the most stable motif [27]. From experimental studies, the inter-layer plane spacing for the stacked PAH structures ranges from 3.5 to 3.9 Å depending on the degree of misalignment of the stacked layer planes [42–45]. Therefore, in terms of the above possible conformations, interatomic distance (d) is measured as the nearest two atoms from different monomers shown in Fig. 2 (a) and compared to an interatomic distance criteria (D). That is, if the interatomic distance is less than the criterion, it is believed that the two monomers belong to one cluster or particle. Here, for example, growth of an incipient soot particle from coronene monomers at 400 K is scrutinized by utilizing criteria of 3, 4 and 5 Å and the results are displayed in Fig. 2 (b). The monomer numbers in the soot particle are quite consistent when employing criteria of 4 and 5 Å compared to that of 3 Å. Moreover, as the intermolecular energy determines the PAH dimerization, binding energy profiles of coronene dimer in center-to-center conformation are tracked as a function of the mass-center-distance of the compounds at temperature ranging from 400 to 2000 K and attached in the supplementary material. By increasing the temperature, changes in the depth and place of the deepest potential well are essentially the same from 400 to 2000 K. The largest depth of intermolecular potential well of PAHs happens when the interatomic distance is about 3–4 Å and PAH dimers are stable around the minimum energies. Hence, criterion of 4 Å is used for our later analysis to distinguish PAH monomers from soot particles or clusters at the temperature range from 400 to 2000 K.

3. Results and discussion

Based on the computational settings described in the previous sections, relationship between the PAH type/mass and temperature as well as evolutions from PAH monomers to incipient soot particles are discussed in this section. Due to the thermal stability of PAHs, decomposition of PAH may only happen at temperatures above 2000 K [46]. Below the decomposition temperature, two distinctive processes are observed, (1) physical nucleation of PAHs into incipient soot particles at low temperatures is discussed in Section 3.1 and, (2) formation of PAH dimers/trimers at elevated temperature is displayed in Section 3.2. Above the decomposition temperature, formation of incipient soot particles through chemical reactions is analyzed in Section 3.3. Finally, in Section 3.4, we summarize the soot nucleation mechanisms in terms of PAH masses and temperatures and compare them with literature data.

3.1. Physical nucleation

Detailed physical nucleation process of coronene at 800 K is displayed in Fig. 3 and the corresponding movie is attached in the supplementary material. Through tracing the conformation evolution, nucleation of incipient soot particles by physical interaction can be well understood. Initially, randomly distributed coronene monomers collide with each other to form PAH dimers. Most of the dimers are in stacks, but a few T-shaped dimers are also observed at time instants b and c (Fig. 3). This is in agreement with the results from Rapacioli et al. [27] who found the stacked PAHs are the most stable. Next, these dimers collide with monomers or dimers to form trimers or tetramers (Fig. 3c). It is noteworthy that one-

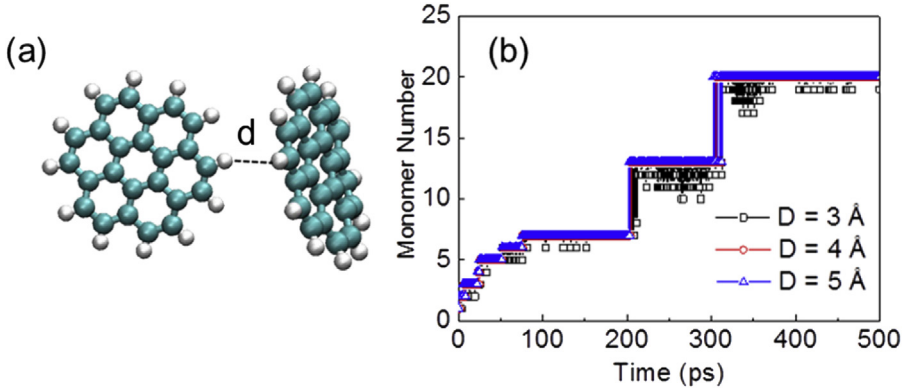

Fig. 2. **(a)** Definition of the interatomic distance (d) between two PAH monomers. **(b)** Growth of monomer number of coronene in an incipient soot particle through physical nucleation at 400 K by changing the interatomic distance criteria (D) of 3, 4 and 5 Å. (A colour version of this figure can be viewed online.)

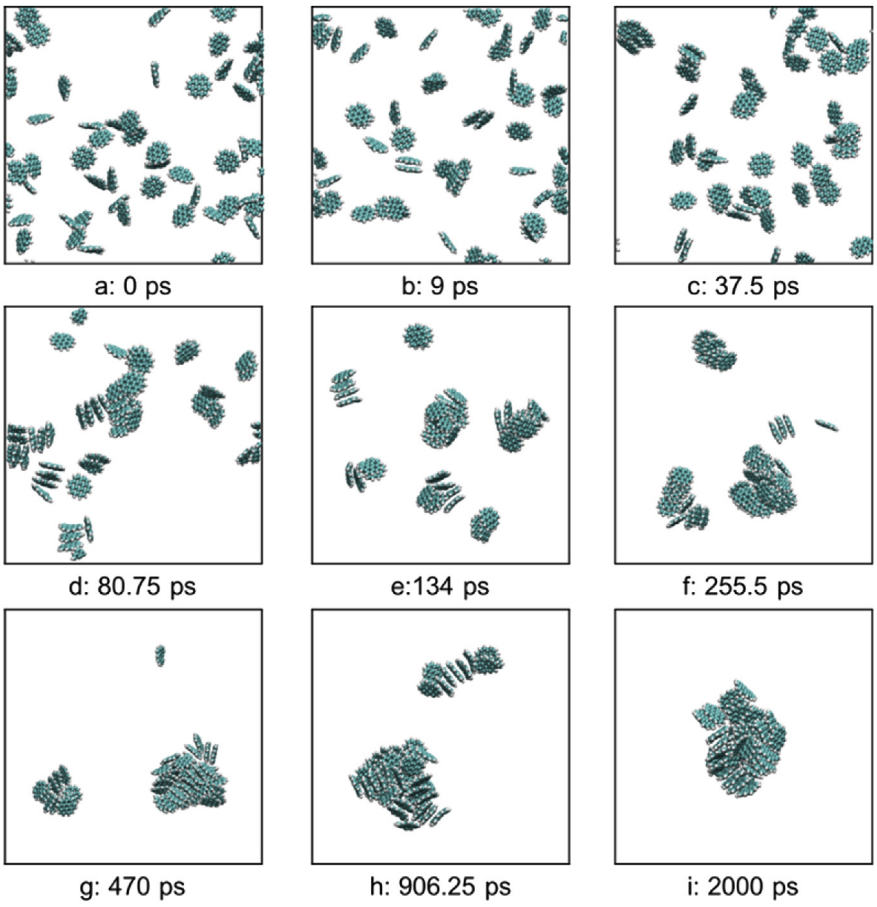

Fig. 3. Snapshots of key stages of the physical nucleation of incipient soot particles from coronene monomers at 800 K. Cyan and white spheres represent carbon and hydrogen atoms, respectively. (A colour version of this figure can be viewed online.)

dimensionally aligned coronene stacks are composed of a maximum of 4–5 monomers at time instants d (Fig. 3). This is consistent with the HR-TEM images of soot particles extracted from diesel engine as the average number of coronene monomer in stacks was reported to be 3.85 [47]. Moreover, T-shaped conformations of 3–4 stacked monomers with one monomer perpendicular to them on the side are also found during this period. Then, at time instant e (Fig. 3), collisions between PAH stacks lead to the formation of incipient soot particles comprised of stacked clusters in three-dimensional shapes. All the above events occur within the initial 150 ps With the increase of the particle size, the particle number density in the system decreases significantly, which leads to the decrease of collision frequency and consequently the rate of soot growth after 150 ps. Later, collisions between soot particles lead to the formation of much larger soot particles as shown from time instants h to i (Fig. 3). The final soot particle tends to be spherical with locally aligned stacked clusters, which is also described as a turbostratic structure [43,45].

3.2. No nucleation

When the temperature increases to 1600 K, the dynamic behaviors of the coronene monomers are recorded and displayed in Fig. 4 and the corresponding movie can be found in the supplementary material. Initially, collisions between PAHs lead to the formation of some dimers and few trimers. However, the dimers or trimers are quite unstable and may dissociate through collisions with surrounding monomers. Throughout the simulation, none of them survives to grow further into incipient soot particles. Since the translational velocity and collision frequency between PAHs at 1600 K are higher than that at 800 K [23], the binding energy between PAHs is not strong enough to stabilize the dimer or trimer from evaporation. This consequently limits the growth from PAH dimers or trimers to incipient soot particles. According to the previous studies [7,12,16], dimerization is regarded as the first nucleation step. In our simulations, we do observe the formation of PAH dimers and trimers, but they cannot grow further into soot particles at elevated temperatures. Therefore, we propose that formation of relatively larger PAH clusters instead of PAH dimers is essential for the continuous soot nucleation and further growth.

3.3. Chemical nucleation

When the temperature increases to above 2000 K, PAHs become thermodynamically unstable and decompose to small radicals or molecules. A detailed dynamic process for PAH fragmentation and soot nucleation, starting from circumcoronene monomers at 2500 K, is shown in Fig. 5. In order to have a better understanding of the fragmentation and reorganization, variations of the number of carbon rings from triangles up to octagon are summarized in Fig. 6. As displayed in Fig. 5, formation of the incipient soot particles through chemical nucleation can be roughly divided into three stages. Initially, from approximately 0 to 1000 ps, PAH dehydrogenation takes place to produce aryl radical from time instants a to b (Fig. 5) - the dissociated H is highlighted in yellow. The aryl radical is unstable and further reaction happens from steps c to d (Fig. 5)

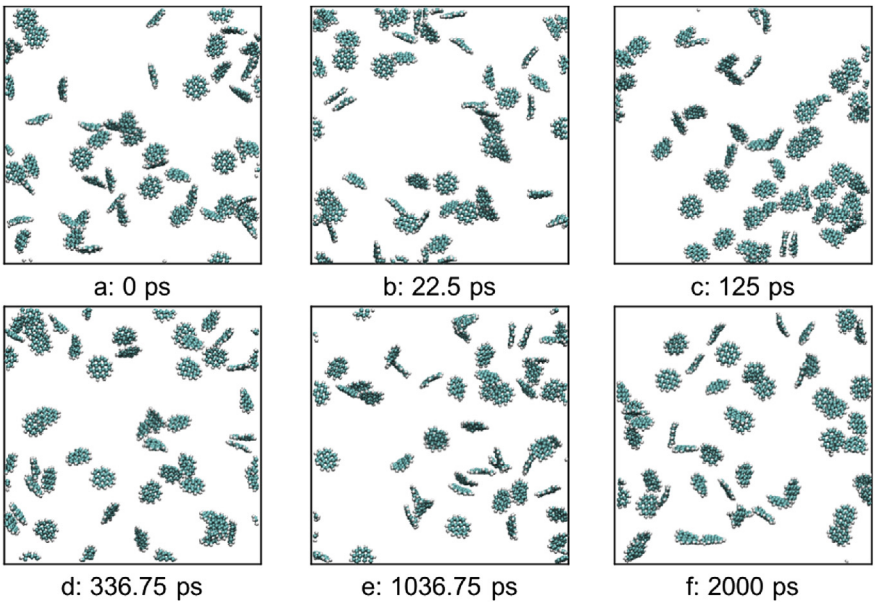

Fig. 4. Snapshots of key stages of the dynamics of coronene monomers at 1600 K. Cyan and white spheres represent carbon and hydrogen atoms, respectively. (A colour version of this figure can be viewed online.)

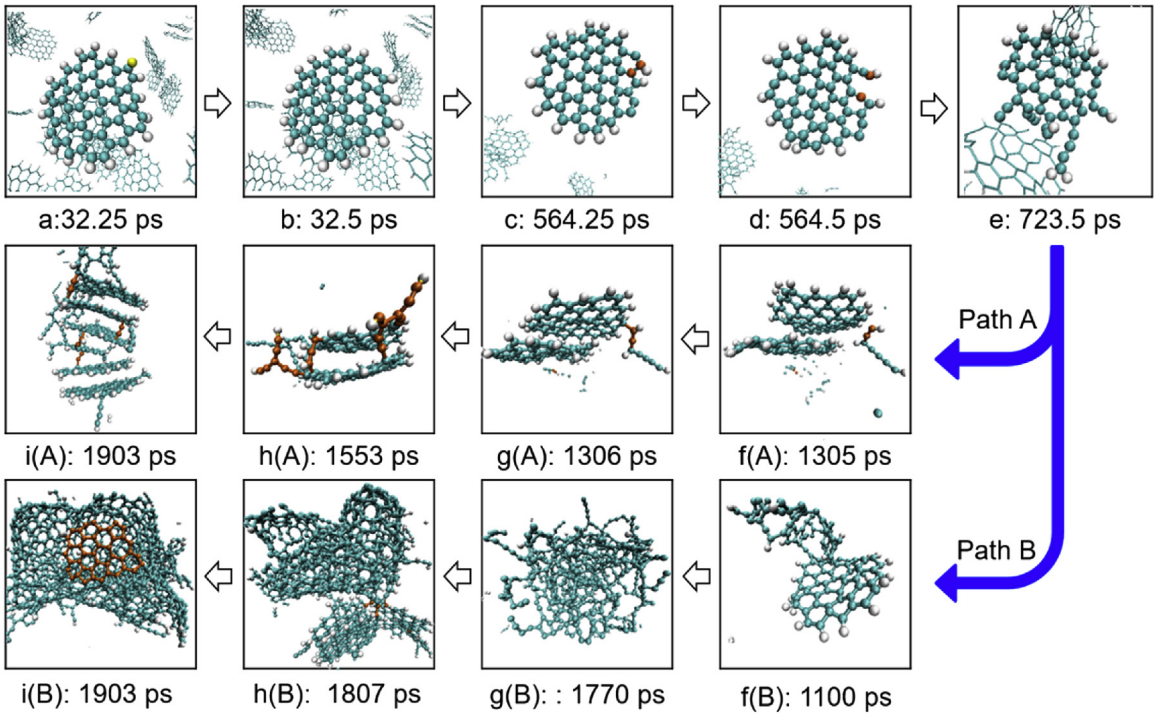

Fig. 5. Snapshots of key stages of PAH fragmentation and soot inception from circumcorenene monomers at 2500 K in path A and path B. Cyan and white spheres represent carbon and hydrogen atoms, respectively. Important carbon and hydrogen atoms are highlighted by orange and yellow. (A colour version of this figure can be viewed online.)

with the scission of C–C bond as the ring opening, which is similar to the β scission in alkanes. Meanwhile, pentagon/heptagon (5/7) pairs appear at the edges of the cracks as a result of edge rearrangements seen at time instant e (Fig. 5), which can also be found in Fig. 6 as the numbers of 5 C-member and 7 C-member rings increase simultaneously during the same period.

Afterwards, from approximately 1000 to 1700 ps, followed by successive C–C bonds splitting, the number of 6 C-member rings decreases dramatically as shown in Fig. 6. Linear or branched polyacetylenic-like radicals or small molecules like C_2H_2 are generated from ring-opening reactions. These radicals help the growth of soot particles in later stages. Our simulation results are in good agreement with theoretical work and experimental results on PAH fragmentation [48]. That is, H- and C_2H_2-loss are the lowest energy channels and all H atoms in a PAH monomer have similar binding energies [49] with values almost independent of the PAH size [50,51]. Further growth from the carbon-based fragments to soot particles is observed in two separated ways as highlighted by

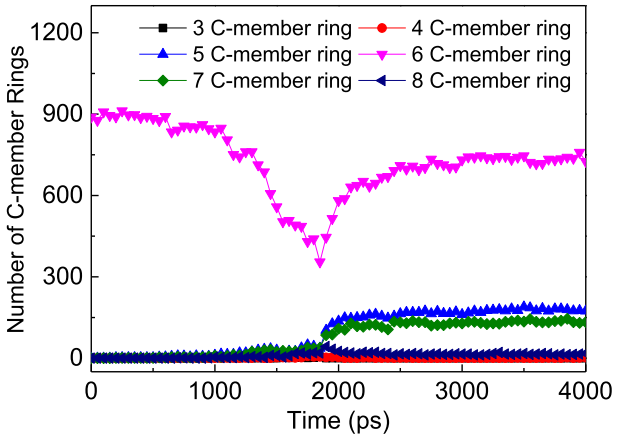

Fig. 6. Ring count statistics during the soot nucleation from circumcoronene monomers as a function of simulation time at 2500 K. (A colour version of this figure can be viewed online.)

path A and path B in Fig. 5. For path A, the polyacetylenic chain radicals connect to the aryl radicals from time instants f (A) to g (A) (Fig. 5). Subsequently, another PAH connects with the aryl radical by H abstraction. These PAH dimers, with the PAH planes parallel to each other, are connected by polyacetylenic chains - highlighted in orange at time instant h (A) (Fig. 5). Further growth from the PAH dimer to PAH cluster is shown at time instant i (A) (Fig. 5). The stacked structure is more like what have been observed during the physical nucleation at low temperatures but connected by 'carbon bridges' on the edge. The connecting covalent bonds are much stronger than the physical interactions, which prevents evaporation at high temperatures. This explains the reason why the number of 6 C-member ring does not decrease to zero before increasing again in Fig. 6 after 1700 ps The other nucleation path, indicated as path B in Fig. 5, is through self-assembly formation of a fullerene-like soot particle. Resulting from the ring-opening and fragmentation process at the initial stage, abundant polyacetylenic linear and branched chains are formed and connect to form long chains with branches as shown in g (B) (Fig. 5). Then the mixed chains connect to some intact PAHs or aryls which act as the nuclei for the reorganization or condensation of the 6-member rings as shown in h (B) (Fig. 5). During this process, the number of 6 C-member ring increases dramatically accompanied by the increase of pentagon/heptagon (5/7) pairs as shown in Fig. 6 after 1700 ps and the orange-highlighted conformation at time instant i (B) (Fig. 5). Moreover, it is observed that some of the 7 C-member rings are occasionally surrounded by more than one 5 C-member rings. This makes the number of 5 C-member ring slightly higher than that of 7 C-member ring in Fig. 6. In addition, the presence of the 5 C-member-ring is reportedly responsible for the bending of the graphene sheets - resulting in the formation of spherical soot particles [52].

3.4. Mechanisms of soot nucleation

In this section, we present a quantitative analysis of the soot inception from different types of PAHs over a range of temperatures. Generally speaking, incipient soot particles are regarded in the size of 1–6 nm [39]. In soot modeling, it is accepted that the mass densities for soot particles comprised of coronene and pyrene are 1.12 and 0.98 g/cm^3 [24], respectively. Hence, an equivalent particle diameter is evaluated from the particle mass and density in our simulations. The number of monomers and the corresponding particle diameters are listed in Fig. 7. For pyrene and coronene particles comprised of 5 monomers, we find that particle diameters are 1.484 and 1.620 nm, respectively. Therefore, if the number of monomers in a soot cluster/particle is larger than 5, nucleation of soot particle is considered to occur.

In a simulation, several soot particles are formed simultaneously. Therefore, only the soot particle comprised of the largest number of PAH monomers is evaluated in our study. Since PAH decomposition and reorganization happen at 2500 K as reported in Section 3.3, an equivalent number of PAH monomers in a soot particle is expressed as the ratio of the particle mass to the corresponding monomer mass. Fig. 8 includes the growth of the largest soot particles from all the six types of PAH at temperatures from 400 to 2500 K and each line is averaged from three independent simulations with different initial conformations. In account of the soot nucleation rate, the initiation and growth at temperatures below 2000 K are significantly different from that at 2500 K. That is, soot inception happens at very initial stage before reaching its plateau at temperatures below 2000 K for each type of PAH. Since PAHs are physically bound in particles below 2000 K, their interactions are occasionally too weak to withstand the collisions from other particles. This consequently results in the break of a particle into smaller ones and the decrease of particle size for circumcoronene at 1600 K as shown in Fig. 8. When the temperature increases to 2500 K, for large PAHs like coronene, ovalene and circumcoronene, steady growth of soot particles starts after ~1500 ps Whereas for naphthalene, anthalene and pyrene, it requires much longer time for the growth to initiate. In addition, growth of soot particle is stage-wise through collision between PAHs or clusters at temperature below 2000 K compared to the gradual trend at 2500 K.

Based on Fig. 8, final sizes of the maximum soot particles formed from each PAH at different temperatures are summarized in Fig. 9, together with the averaged C/H ratios in the corresponding particles. For anthracene and pyrene, we added simulations at 600 K to find more feasible temperatures for soot nucleation. The interplay between the temperature and the size of the maximum soot particle for all the six types of PAHs is consistent. That is, at temperatures below 2000 K, size of the maximum soot particle first increases and then decreases with the increase of temperatures. However, when the temperature rises to 2500 K, sizes of soot particles increase once more. In addition, for each type of PAH at temperatures below 2000 K, the C/H ratios in the maximum soot particles maintain the same as the corresponding PAH monomers. However, at 2500 K, the C/H ratios increase sharply for all the PAHs, illustrating the dehydrogenation and graphitization during the soot nucleation. It is in good agreement with the previous studies as mature soot particles grows by the addition of mass and is accompanied by graphitization [39,46,53,54].

Finally, according to the behaviors of different types of PAHs at

Monomer number	Diameter (nm)	
	Pyrene	Coronene
5	1.484	1.620
10	1.870	2.041
15	2.141	2.336
20	2.356	2.571
50	3.198	3.490

Fig. 7. The number of PAH monomer, PAH type and the correspondingly equivalent particle diameter of incipient soot particle.

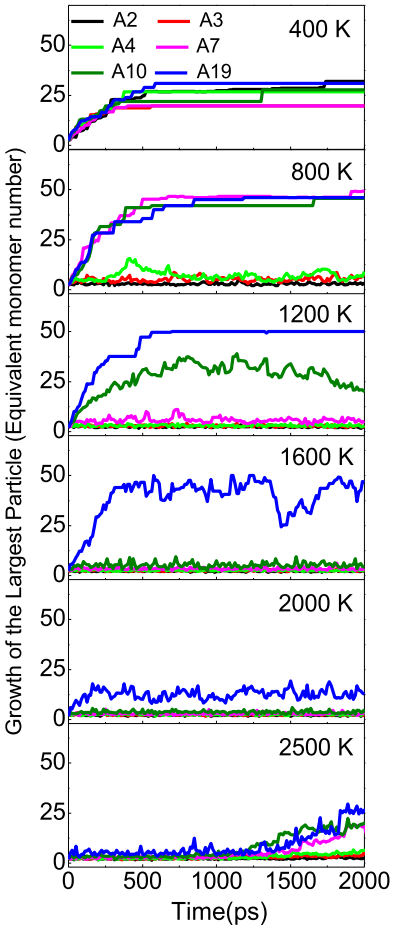

Fig. 8. Growth of the maximum soot particles comprised of PAH monomers of naphthalene (A2), anthracene (A3), pyrene (A4), coronene (A7), ovalene (A10) and circumcoronene (A19) at temperatures ranging from 400 to 2500 K. (A colour version of this figure can be viewed online.)

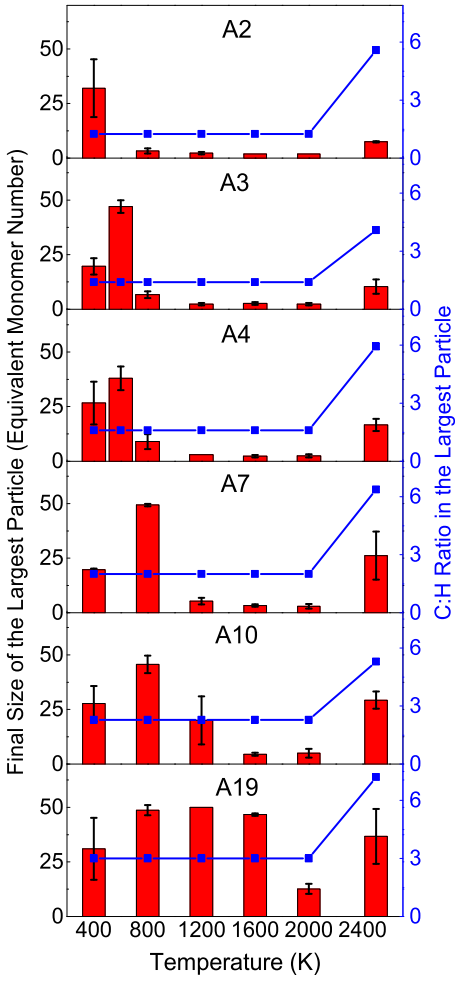

Fig. 9. Equivalent monomer number (left axis, colored in red and black columns with error bars) and C/H ratio (right axis, colored in blue closed squares) in the maximum soot particle comprising naphthalene (A2), anthracene (A3), pyrene (A4), coronene (A7), ovalene (A10) and circumcoronene (A19) monomers as a function of temperature from 400 to 2500 K. (A colour version of this figure can be viewed online.)

varied temperatures, we summarize the temperature and PAH mass dependent homogenous soot nucleation mechanisms in Fig. 10. Physical nucleation of incipient soot particles is strongly dependent on the temperature as well as PAH mass as indicated in Figs. 8 and 9. At low temperatures, e.g., 400 K, physical nucleation of incipient soot particles is applicable to all the six types of PAHs through step-wise addition of monomers or clusters and forming incipient soot particles comprised of stacks in different orientations. With the increase of temperature, the feasibility to form incipient soot particles decreases with the decrease of PAH mass. Specifically, naphthalene, anthracene and pyrene, with 2-, 3- and 4-numbered aromatic rings, cannot grow into incipient soot particles at temperatures above 800 K. Instead, predominant formation of dimers, trimers or tetramers is observed. When the temperature rises to 1200 K and above, coronene with 7-numbered aromatic rings can no longer form incipient soot particles. A similar phenomenon happens for ovalene at temperatures above 1600 K. Only circumcoronene, with 19-numbered aromatic rings, is found to form incipient soot particles even at 2000 K. Details of the physical nucleation and no nucleation for all the PAHs are in the way as shown in Figs. 3 and 4. The boiling/sublimation temperatures of naphthalene, anthracene, pyrene and coronene [55] are consistent with the physical nucleation threshold line from the ReaxFF MD simulations. For coronene, ovalene and circumcoronene, we also compare the highest temperatures for feasible homomolecular

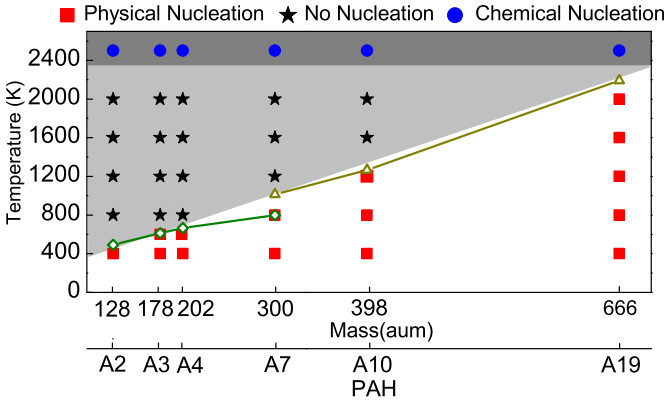

Fig. 10. Nucleation mechanisms of PAHs in homogenous systems. The closed red squares, black stars and blue circles represent physical nucleation, no nucleation and chemical nucleation, respectively. The open olive diamonds and tan triangles are from the previous studies on the PAH boiling/sublimation temperatures [55] and equilibrium temperatures for PAH dimerization [7], respectively. Soot nucleation mechanisms can be roughly divided into three regions according to PAH masses and temperatures, (i) physical nucleation (white), (ii) no nucleation (light grey) and (iii) chemical nucleation (dark grey). (A colour version of this figure can be viewed online.)

dimerization from the equilibrium constants calculation as shown in Fig. 10. Findings in our simulations are highly consistent with these theoretical results. That is, below the boiling temperature or dimerization temperature, physical nucleation of PAHs leads to the formation of incipient soot particles; above the boiling temperatures, PAHs cannot condense to form incipient soot particles.

At high temperatures (2500 K), PAHs are thermodynamically unstable [46] and growth of incipient soot particles results from chemical reactions. Though we observed chemical events took place at 2500 K on a ReaxFF MD simulation of nanosecond scale – on experimental time-scales the temperature for chemical nucleation may be substantially lower. Before soot nucleation, decomposition and fragmentation of PAHs initiated. For naphthalene, anthracene and pyrene, we only observe the soot growth in the way of path B (Fig. 5), that is, through the self-assembly formation of fullerene-like soot particles. This can be understood from the fact that the small PAHs cannot survive the decomposition stage and most of the PAHs experience the ring-opening processes before carbon-based chain radicals connect to them. The above process follows the bottom-up mechanisms, as fullerene-like soot particles are considered to be formed from polyacetylenic linear and branched chains [56] instead of directly being formed from a "two-dimensional" PAHs curve [15]. Chuvilin et al.'s [56] experiments indicated that direct formation of a fullerene-like structure from graphene has a relatively narrow range of diameters averaging about 1 nm, corresponding to 60–100 carbon atoms. In our simulation, the largest PAH monomer (circumcoronene) contains 54 carbon atoms, which is still smaller than the critical size. Moreover, the peak concentrations of PAHs in premixed sooting flames drop by roughly one order of magnitude with the increment of two pericondensed rings [7]. In other words, the existence of PAH monomers with carbon numbers larger than 60 is extremely rare.

4. Conclusions

In this paper, nucleation of incipient soot particles from simple to complex PAHs is studied using ReaxFF MD simulations. PAH monomers constituted of 2-, 3-, 4-, 7-, 10-, and 19-numbered aromatic rings, namely naphthalene, anthracene, pyrene, coronene, ovalene and circumcoronene are studied. Both qualitative and quantitative investigations into the formation of incipient soot particles from these PAHs are conducted over the typical temperatures in high-temperature aerosol environment ranging from 400 to 2500 K. Three distinctive regimes are identified for soot formation as a function of temperature and PAH mass. At low temperatures (e.g., 400 K), all the PAHs experience physical nucleation and form incipient particles comprising stacked clusters with different orientations. With the increase of temperature, PAH dimers and trimers are formed but these do not grow further into incipient soot particles. Large PAH monomers have a higher possibility of growing into incipient soot particles than small PAHs due to stronger physical interactions. The threshold lines dividing the physical nucleation and no nucleation regimes are identified for each type of PAH, which agree well with the boiling/sublimation and feasible dimerization temperatures of the PAHs. At 2500 K, PAHs grow to incipient soot particles by the chemical mechanism. PAH monomers firstly experience ring opening with the abstraction of H, C_2H_2 and polyacetylenic chain radicals. For large PAHs like coronene, ovalene and circumcoronene, polyacetylenic chain radicals help to connect them to form soot particles in stacked structures with 'carbon bridges' on the edge. Additionally, the dissociated radicals connect with each other and nucleate to form fullerene-like soot particles for all types of PAHs. Results from this study indicate the importance of temperature on the mechanisms of soot nucleation from PAHs and provide insight for developing a more accurate soot nucleation model by considering temperature and PAH mass together with physical and chemical effects.

Acknowledgement

Support from Major Programmes of the National Science Foundation of China (Grant No. 51390493 and Grant No. 91441120), the China Scholarship Council and the Center for Combustion Energy at Tsinghua University is gratefully acknowledged. The simulations were performed on ARCHER funded under the EPSRC project "UK Consortium on Mesoscale Engineering Sciences (UKCOMES)" (Grant No. EP/L00030X/1). ACTvD acknowledges funding from NSF grant# 1462980. The authors are particularly grateful to Prof. Richard A Yetter at Penn State for helpful discussions.

Appendix A. Supplementary data

Supplementary data related to this article can be found at http://dx.doi.org/10.1016/j.carbon.2017.06.009.

References

[1] S. Li, Y. Ren, P. Biswas, S.D. Tse, Flame aerosol synthesis of nanostructured materials and functional devices: processing, modeling, and diagnostics, Prog. Energy Combust. Sci. 55 (2016) 1–59, http://dx.doi.org/10.1016/j.pecs.2016.04.002.
[2] A.K. Geim, K.S. Novoselov, The rise of graphene, Nat. Mater 6 (2007) 183–191, http://dx.doi.org/10.1038/nmat1849.
[3] K. Okude, K. Mori, S. Shiino, T. Moriya, Premixed compression ignition (PCI) combustion for simultaneous reduction of NOx and soot in diesel engine, SAE Trans. 113 (2004) 1002–1013, http://dx.doi.org/10.4271/2004-01-1907.
[4] H. Horvath, Atmospheric light absorption—a review, Atmos. Environ. Part A. Gen. Top. 27 (1993) 293–317, http://dx.doi.org/10.1016/0960-1686(93)90104-7.
[5] K.S. Johnson, B. Zuberi, L.T. Molina, M.J. Molina, M.J. Iedema, J.P. Cowin, D.J. Gaspar, C. Wang, A Laskin, Processing of soot in an urban environment: case study from the Mexico City Metropolitan Area, Atmos. Chem. Phys. 5 (2005) 3033–3043, http://dx.doi.org/10.5194/acpd-5-5585-2005.
[6] M. Matti Maricq, Chemical characterization of particulate emissions from diesel engines: a review, J. Aerosol Sci. 38 (2007) 1079–1118, http://dx.doi.org/10.1016/j.jaerosci.2007.08.001.
[7] H. Wang, Formation of nascent soot and other condensed-phase materials in flames, Proc. Combust. Inst. 33 (2011) 41–67, http://dx.doi.org/10.1016/j.proci.2010.09.009.
[8] J.B. Howard, Fullerenes formation in flames, Symp. Combust. 24 (1992) 933–946, http://dx.doi.org/10.1016/S0082-0784(06)80111-6.
[9] P. Gerhardt, S. Löffler, K.H. Homann, The formation of polyhedral carbon ions in fuel-rich acetylene and benzene flames, Symp. Combust. 22 (1989) 395–401, http://dx.doi.org/10.1016/S0082-0784(89)80046-3.
[10] M. Frenklach, Reaction mechanism of soot formation in flames, Phys. Chem. Chem. Phys. 4 (2002) 2028–2037, http://dx.doi.org/10.1039/b110045a.
[11] J.D. Herdman, J.H. Miller, Intermolecular potential calculations for polynuclear aromatic hydrocarbon clusters, J. Phys. Chem. A 112 (2008) 6249–6256, http://dx.doi.org/10.1021/jp800483h.
[12] C.A. Schuetz, M. Frenklach, Nucleation of soot: molecular dynamics simulations of pyrene dimerization, Proc. Combust. Inst. 29 (2002) 2307–2313, http://dx.doi.org/10.1016/S1540-7489(02)80281-4.
[13] A. Violi, A.F. Sarofim, G.A. Voth, Kinetic Monte carlo–molecular dynamics approach to model soot inception, Combust. Sci. Technol. 176 (2004) 991–1005, http://dx.doi.org/10.1080/00102200490428594.
[14] H. Richter, J.B. Howard, Formation of Polycyclic Aromatic Hydrocarbons and Their Growth to Soot - a Review of Chemical Reaction Pathways, 2000, http://dx.doi.org/10.1016/S0360-1285(00)00009-5.
[15] K.-H. Homann, Fullerenes and soot formation - new pathways to large particles in flames, Angew. Chem. Int. Ed. 37 (1998) 2435–2451, http://dx.doi.org/10.1002/(SICI)1521-3773(19981002)37, 18<2434::AID-ANIE2434>3.0.CO;2-L.
[16] S. Deng, M.E. Mueller, Q.N. Chan, N.H. Qamar, B.B. Dally, Z.T. Alwahabi, G.J. Nathan, Hydrodynamic and chemical effects of hydrogen addition on soot evolution in turbulent nonpremixed bluff body ethylene flames 0 (2016) 1–8, http://dx.doi.org/10.1016/j.proci.2016.09.004.
[17] N.A. Eaves, S.B. Dworkin, M.J. Thomson, Assessing relative contributions of PAHs to soot mass by reversible heterogeneous nucleation and condensation, Proc. Combust. Inst. 36 (2017) 935–945, http://dx.doi.org/10.1016/j.proci.2016.06.051.
[18] H.B. Zhang, X. You, H. Wang, C.K. Law, Dimerization of polycyclic aromatic hydrocarbons in soot nucleation, J. Phys. Chem. A 118 (2014) 1287–1292,

http://dx.doi.org/10.1021/jp411806q.
[19] H. Nagai, M. Nakano, K. Yoneda, R. Kishi, H. Takahashi, A. Shimizu, T. Kubo, K. Kamada, K. Ohta, E. Botek, B. Champagne, Signature of multiradical character in second hyperpolarizabilities of rectangular graphene nanoflakes, Chem. Phys. Lett. 489 (2010) 212–218, http://dx.doi.org/10.1016/j.cplett.2010.03.013.
[20] S.H. Chung, A. Violi, Peri-condensed aromatics with aliphatic chains as key intermediates for the nucleation of aromatic hydrocarbons, Proc. Combust. Inst. 33 (2011) 693–700, http://dx.doi.org/10.1016/j.proci.2010.06.038.
[21] P. Elvati, A. Violi, Thermodynamics of poly-aromatic hydrocarbon clustering and the effects of substituted aliphatic chains, Proc. Combust. Inst. 34 (2013) 1837–1843, http://dx.doi.org/10.1016/j.proci.2012.07.030.
[22] A. Violi, S. Izvekov, Soot primary particle formation from multiscale coarse-grained molecular dynamics simulation, Proc. Combust. Inst. 31 (2007) 529–537, http://dx.doi.org/10.1016/j.proci.2006.07.240.
[23] T.S. Totton, A.J. Misquitta, M. Kraft, A quantitative study of the clustering of polycyclic aromatic hydrocarbons at high temperatures, Phys. Chem. Chem. Phys. 14 (2012) 4081–4094, http://dx.doi.org/10.1039/c2cp23008a.
[24] T.S. Totton, D. Chakrabarti, A.J. Misquitta, M. Sander, D.J. Wales, M. Kraft, Modelling the internal structure of nascent soot particles, Combust. Flame 157 (2010) 909–914, http://dx.doi.org/10.1016/j.combustflame.2009.11.013.
[25] A. Raj, M. Sander, V. Janardhanan, M. Kraft, A study on the coagulation of polycyclic aromatic hydrocarbon clusters to determine their collision efficiency, Combust. Flame 157 (2010) 523–534, http://dx.doi.org/10.1016/j.combustflame.2009.10.003.
[26] D. Chen, T.S. Totton, J.W.J. Akroyd, S. Mosbach, M. Kraft, Size-dependent melting of polycyclic aromatic hydrocarbon nano-clusters: a molecular dynamics study, Carbon N. Y. 67 (2014) 79–91, http://dx.doi.org/10.1016/j.carbon.2013.09.058.
[27] M. Rapacioli, F. Calvo, F. Spiegelman, C. Joblin, D.J. Wales, Stacked clusters of polycyclic aromatic hydrocarbon molecules, J. Phys. Chem. A 109 (2005) 2487–2497, http://dx.doi.org/10.1021/jp046745z.
[28] M. Sirignano, A. Collina, M. Commodo, P. Minutolo, A. D'Anna, Detection of aromatic hydrocarbons and incipient particles in an opposed-flow flame of ethylene by spectral and time-resolved laser induced emission spectroscopy, Combust. Flame 159 (2012) 1663–1669, http://dx.doi.org/10.1016/j.combustflame.2011.11.005.
[29] A.C.T. van Duin, S. Dasgupta, F. Lorant, W.A. Goddard III, ReaxFF: a reactive force field for hydrocarbons, J. Phys. Chem. A 105 (2001) 9396–9409, http://dx.doi.org/10.1021/jp004368u.
[31] D.W. Brenner, Empirical potential for hydrocarbons for use in simulating the chemical vapor deposition of diamond films, Phys. Rev. B 42 (1990) 9458–9471, http://dx.doi.org/10.1103/PhysRevB.42.9458.
[32] J. Tersoff, Empirical interatomic potential for carbon, with applications to amorphous carbon, Phys. Rev. Lett. 61 (1988) 2879–2882, http://dx.doi.org/10.1103/PhysRevLett.61.2879.
[33] S. Goverapet Srinivasan, A.C.T. Van Duin, P. Ganesh, Development of a ReaxFF potential for carbon condensed phases and its application to the thermal fragmentation of a large fullerene, J. Phys. Chem. A 119 (2015) 571–580, http://dx.doi.org/10.1021/jp510274e.
[34] U. Khalilov, A. Bogaerts, E.C. Neyts, Atomic scale simulation of carbon nanotube nucleation from hydrocarbon precursors, Nat. Commun. 6 (2015) 10306, http://dx.doi.org/10.1038/ncomms10306.
[35] K. Yoon, A. Ostadhossein, A.C.T. Van Duin, Atomistic-scale simulations of the chemomechanical behavior of graphene under nanoprojectile impact, Carbon N. Y. 99 (2016) 58–64, http://dx.doi.org/10.1016/j.carbon.2015.11.052.
[36] K. Yoon, A. Rahnamoun, J.L. Swett, V. Iberi, D.A. Cullen, I.V. Vlassiouk, A. Belianinov, S. Jesse, X. Sang, O.S. Ovchinnikova, A.J. Rondinone, R.R. Unocic, A.C.T. Van Duin, Atomistic-scale simulations of defect formation in graphene under noble gas ion irradiation, ACS Nano 10 (2016) 8376–8384, http://dx.doi.org/10.1021/acsnano.6b03036.
[37] R.I. Singh, A.M. Mebel, M. Frenklach, Oxidation of graphene-edge six- and five-member rings by molecular oxygen, J. Phys. Chem. A 119 (2015) 7528–7547, http://dx.doi.org/10.1021/acs.jpca.5b00868.
[38] J. Happold, H.-H. Grotheer, M. Aigner, Soot precursors consisting of stacked pericondensed PAHs, in: H. Bockhorn, A. D'Anna, A.F. Sarofirm, H. Wang (Eds.), Proceedings of an International Workshop Held in Villa Orlandi, Anacapri, Karlsruhe University Press, May 13–16, 2007, pp. 275–285.
[39] H.A. Michelsen, Probing soot formation, chemical and physical evolution, and oxidation : a review of in situ diagnostic techniques and needs, Proc. Combust. Inst. 0 (2016) 1–19, http://dx.doi.org/10.1016/j.proci.2016.08.027.
[40] S. Plimpton, Fast parallel algorithms for short-range molecular-dynamics, J. Comput. Phys. 117 (1995) 1–19, http://dx.doi.org/10.1006/jcph.1995.1039.
[41] W. Humphrey, A. Dalke, K. Schulten, VMD: visual molecular dynamics, J. Mol. Graph 14 (1996) 33–38, http://dx.doi.org/10.1016/0263-7855(96)00018-5.
[42] C.R. Kinney, R.C. Nunn, P.L. Walker, Carbonization of anthracene and graphitization of anthracene carbons, Ind. Eng. Chem. 49 (1957) 880–884, http://dx.doi.org/10.1021/ie50569a034.
[43] R.D. Heidenreich, W.M. Hess, L.L. Ban, A test object and criteria for high resolution electron microscopy, J. Appl. Crystallogr. 1 (1968) 1–19, http://dx.doi.org/10.1107/S0021889868004930.
[44] T. Edstrom, I.C. Lewis, Chemical structure and graphitization: X-ray diffraction studies of graphites derived from polynuclear aromatics, Carbon N. Y. 7 (1969) 85–91, http://dx.doi.org/10.1016/0008-6223(69)90008-6.
[45] P. Marsh, A. Voet, T. Mullens, Electron micrography of interplanar spacings in carbon blacks, Rubber Chem. Technol. 43 (1970) 470–481, http://dx.doi.org/10.5254/1.3547269.
[46] S.E. Stein, A. Fahr, High-temperature stabillties of hydrocarbons, Am. Chem. Soc. 89 (1985) 3114–3125, http://dx.doi.org/10.1021/j100263a027.
[47] S. Mosbach, M.S. Celnik, A. Raj, M. Kraft, H.R. Zhang, S. Kubo, K.O. Kim, Towards a detailed soot model for internal combustion engines, Combust. Flame 156 (2009) 1156–1165, http://dx.doi.org/10.1016/j.combustflame.2009.01.003.
[48] A.I.S. Holm, H.A.B. Johansson, H. Cederquist, H. Zettergren, Dissociation and multiple ionization energies for five polycyclic aromatic hydrocarbon molecules, J. Chem. Phys. 134 (2011) 44301, http://dx.doi.org/10.1063/1.3541252.
[49] K. Fujiwara, A. Harada, J. Aihara, CH bond dissociation energies of polycyclic aromatic hydrocarbon molecular cations: theoretical interpretation of the (M-1)+ peak in the mass spectra, J. Mass Spectrom. 31 (1996) 1216–1220, http://dx.doi.org/10.1002/(SICI)1096-9888(199611)31, 11.
[50] R.H. Chen, S.A. Kafafi, S.E. Stein, Reactivity of polycyclic aromatic aryl radicals, J. Am. Chem. Soc. 111 (1989) 1418–1423, http://dx.doi.org/10.1021/ja00186a041.
[51] C. Lifshitz, Energetics and dynamics through time-resolved measurements in mass spectrometry: aromatic hydrocarbons, polycyclic aromatic hydrocarbons and fullerenes, Int. Rev. Phys. Chem. 16 (1997) 113–139, http://dx.doi.org/10.1080/014423597230235.
[52] R. Whitesides, M. Frenklach, Detailed kinetic Monte Carlo simulations of graphene-edge growth, J. Phys. Chem. A 114 (2010) 689–703, http://dx.doi.org/10.1021/jp906541a.
[53] R.A. Dobbins, R.A. Fletcher, W. Lu, Laser microprobe analysis of soot precursor particles and carbonaceous soot, Combust. Flame 100 (1995) 301–309, http://dx.doi.org/10.1016/0010-2180(94)00047-V.
[54] R.A. Dobbins, R.A. Fletcher, H.C. Chang, The evolution of soot precursor particles in a diffusion flame, Combust. Flame 115 (1998) 285–298, http://dx.doi.org/10.1016/S0010-2180(98)00010-8.
[55] C.M. White, Prediction of the boiling point, heat of vaporization, and vapor pressure at various temperatures, J. Chem. Eng. Data 31 (1986) 198–203, http://dx.doi.org/10.1021/je00044a020.
[56] A. Chuvilin, U. Kaiser, E. Bichoutskaia, N. a N. Besley, A.N. Khlobystov, Direct transformation of graphene to fullerene, Nat. Chem. 2 (2010) 450–453, http://dx.doi.org/10.1038/nchem.644.